Electrical and thermal control of magnetic coercive field in ferromagnetic/ferroelectric heterostructures

Zhiguang Wang,[1,*] Yue Zhang,[1] Ravindranath Viswan,[1] Yanxi Li,[1] Haosu Luo,[2] Jiefang Li,[1] and D. Viehland[1]

[1]*Department of Materials Science and Engineering, Virginia Tech, Blacksburg, Virginia 24061, USA*

[2]*State Key Laboratory of High Performance Ceramics and Superfine Microstructure, Shanghai Institute of Ceramics, Chinese Academy of Sciences, Shanghai 201800, China*

(Received 24 September 2013; revised manuscript received 9 December 2013; published 13 January 2014)

We report the growth of ferromagnetic epitaxial $CoFe_2O_4$ (CFO) thin films on 011-oriented tetragonal-structured $0.62Pb(Mg,Nb)O_3$-$0.38PbTiO_3$ single crystal substrates. In the substrates, electric field-induced polarization reorientation resulted in maximum strains of -1.3% and 0.64% along in-plane 100 and along in-plane $0\bar{1}1$, respectively. As a consequence, in the CFO films, irreversible magnetic coercive field changes of 580, -510, and -220 Oe were observed along in-plane 100 and $0\bar{1}1$ and out-of-plane 011, respectively, after electric field poling. After annealing at 470 K, the substrate depoled, and both the magnetic coercive fields and the remnant magnetizations along the three directions recovered their original values.

DOI: 10.1103/PhysRevB.89.035118 PACS number(s): 75.85.+t, 77.55.Nv, 85.75.−d, 85.80.Jm

I. INTRODUCTION

Cobalt ferrite or $CoFe_2O_4$ (CFO) has been the subject of many investigations because of its large magnetostriction, magnetocrystalline anisotropy, and unique nonlinear spin-wave properties. These properties promise applications in data storage, sensors, drug delivery, and imaging.[1–6] The magnetic coercive field (H_c) is one of the most important parameters for these applications:[7] for example, magnetic materials with high coercivity and perpendicular magnetic anisotropy have been used in ultra-high-density recording.[8,9]

There are three principle ways to control the magnetic coercive field in ferromagnetic materials. First, architecture design and fabrication of magnetic nanostructures with different aspect ratios and particle sizes results in dramatic changes in H_c, due to magnetic shape anisotropy and quantum effects.[10] Second, the temperature dependence of H_c enables laser heat-assisted magnetic perpendicular recording (HAMR), where H_c can be dramatically decreased as the bit area is heated to the magnetic Curie temperature.[11] Third, elastic strain has proven to be effective in the control of H_c,[12,13] where the magnetic shape anisotropy can be controlled only during the fabrication process. High-temperature treatment of a memory cell induces error in the writing process, and the writing rate is restricted by the cooling rate of the heated bit area.[14,15] However, elastic strain control of H_c can be realized through magnetoelectric exchange, where the electric and magnetic orders are coupled to each other. Electric field-tunable H_c promises memory devices with a high recording density and high operating rate, as well as low energy consumption.[16]

Ferromagnetic thin films have previously been deposited on piezoelectric single crystals.[17,18] However, these prior studies focused on PMN-xPT crystals whose compositions were in the vicinity of the morphotropic phase boundary (MPB), which was selected in order to take advantage of their high piezoelectric coefficients. Renault *et al.*[19] systematically studied the temperature range of existence of the electric field-induced orthorhombic (O) phase in $Pb(Zn_{1/3}Nb_{2/3})_{0.955}Ti_{0.045}O_3$, which clearly confirmed that the electric field along 101 can rotate the spontaneous polarizations into the ones that along 101, forming a monodomain O phase. Franzbach *et al.*[20] systematically studied the value of the electric field for tetragonal (T) phase-to-O phase transformation, which showed a linear relationship with temperature. As for PMN-PT, we have previously reported the electric field phase transition in the vicinity of MPB, where electric field-induced strains smaller than 0.4% were observed.[21–23] Alternatively, much larger strains could be induced by polarization reorientation in T-phase PMN-PT, where the unit cells tend to align their long axes along the external electric field.[24] The induced strain ε is proportional to the difference between lattice parameters of the long and short axes: i.e., $\varepsilon = (c - a)/a$.[25] A step decrease in the magnetization by ~65% has previously been reported for $(La,Sr)MnO_3$ films on $BaTiO_3$ (BTO, T phase) heterostructures.[26] The value of ε in T-phase PMN-PT can reach 2%, whereas that of BTO is only 1.1%.[27,28] Accordingly, a much larger polarization reorientation-induced strain can be expected in T-structured PMN-PT single crystals.

Here, we report epitaxial growth of CFO thin films on 011-oriented $0.62Pb(Mg,Nb)O_3$-$0.38PbTiO_3$ (PMN-38PT) single crystal substrates, along with systematic studies of the change in both the remnant magnetization (M_r) and H_c due to the uniaxial strain induced by an electric field applied to the substrate along the in-plane direction.

II. EXPERIMENTAL DETAILS

PMN-38PT substrates of $5 \times 5 \times 0.5$ mm with a T structure at room temperature were grown at the Shanghai Institute of Ceramics Chinese Academy Sciences by a Bridgman method. The thickness of the CFO films was 400 nm after 1-h deposition by pulsed laser deposition (KrF excimer laser, $\lambda = 248$ nm) at 800 °C. The laser was focused to a spot size of ~2 mm^2 and was incident on the surface of the target using an energy density of 6 J/cm^2. The distance between the substrate and the target was 6 cm, and the base vacuum of the chamber was 10^{-6} torr. During film deposition, the oxygen pressure was 90 mtorr. The crystal structure of the films was determined using a Philips X'pert high-resolution x-ray diffractometer (XRD) with an x-ray wavelength of Cu $K\alpha = 1.5406$ Å. Magnetic hysteresis (M-H) loops were measured with a Lakeshore 7300 series vibrating sample magnetometer system at room temperature,

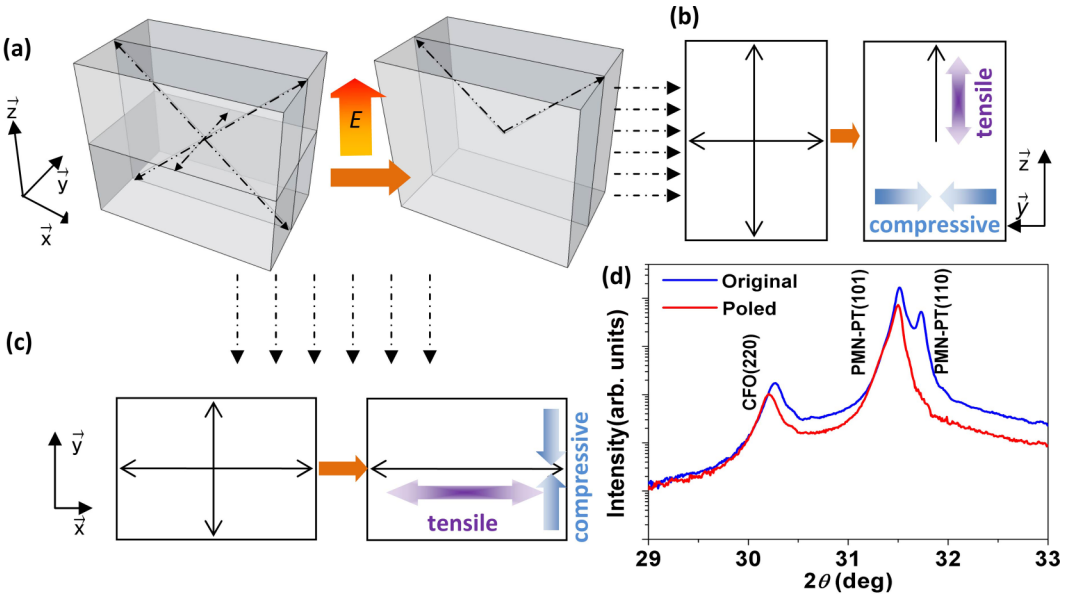

FIG. 1. (Color online) Schematic of polarization reorientation-induced uniaxial strains in both in-plane and out-of-plane directions. (a) Six possible polarization orientations in T-phase PMN-PT, which are degenerated into two upward ones by E along the out-of-plane direction. Uniaxial strains within (b) $(\vec{y},\vec{z})$ planes and (c) $(\vec{x},\vec{y})$ planes. (d) XRD of CFO thin films on poled and unpoled 011-oriented PMN-PT substrate.

where the samples were connected to a Bertan high-voltage power supply (210-20R) in order to apply electric fields.

III. RESULTS AND DISCUSSION

Figure 1 illustrates the polarization reorientation-induced uniaxial strains within both $(\vec{y},\vec{z})$ and $(\vec{x},\vec{y})$ planes. The T phase of PMN-38PT has six possible polarization orientations, as shown in Fig. 1(a). Application of electric field (E) along the out-of-plane direction will align these orientations to being closer to that of the direction of E. Since the crystal lattice parameters of PMN-38PT are longer along the polar direction, polarization reorientation will induce a large strain, which can then be transmitted to an epitaxially grown film.[29,30] In the $(\vec{y},\vec{z})$ plane, there are six possible polarization projections along $\vec{y}$ and $\vec{z}$ before application of E. However, these six will be degenerated into two possible orientations that are directed upward after application of a sufficiently large E along the out-of-plane direction. This will result in a polarization projection along only $\vec{z}$, as shown in Fig. 1(b). Accordingly, tensile and compressive strains can be expected along $\vec{z}$ and $\vec{y}$, respectively. In the $(\vec{x},\vec{y})$ plane, under application of E, the four possible polarization projections will be degenerated into two along $\vec{x}$. This will result in tensile and compressive strains along $\vec{x}$ and $\vec{y}$, respectively, as shown in Fig. 1(c). Two types of domains can be identified based on the d spacing between adjacent planes along the out-of-plane direction: domain I, whose polarization is along $\vec{y}$ with $d_1 = \frac{\sqrt{2}a}{2}$, and domain II, whose polarization is not along $\vec{y}$ with $d_2 = \frac{a\times c}{\sqrt{a^2+c^2}}$, where a and c are the T crystal lattice parameters and d_1 and d_2 are the distances between adjacent planes along $\vec{z}$. Figure 1(d) shows a comparison of XRD line scans before and after poling: the (110) peak is from domain I, whereas the (101) one is from domain II. After poling the substrate, the (110) peak disappeared. This demonstrates a complete domain I $\rightarrow$ domain II transformation under E. The crystal lattice parameters of the T structure were calculated from the 2θ positions and determined to be $(a, c) = (3.980, 4.031$ Å$)$.[30]

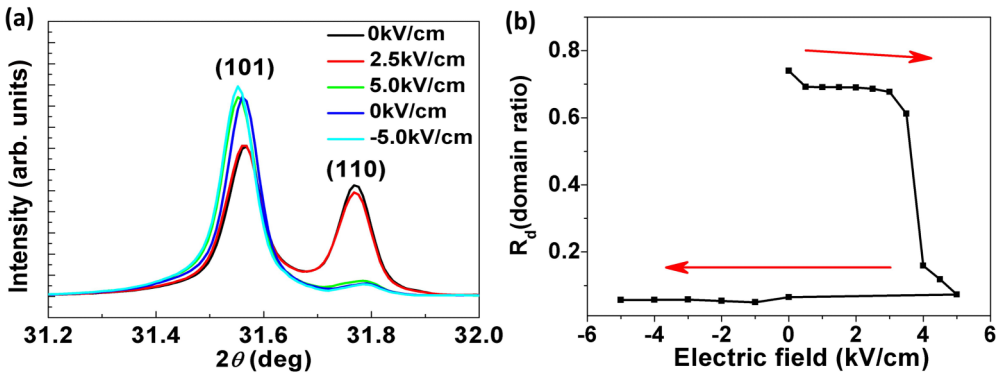

FIG. 2. (Color online) (a) XRD of PMN-38PT substrate under different electric fields. (b) Electric field dependence of the domain I-to-domain II ratio, calculated by comparisons of diffraction intensities of the (101) and (110) peaks.

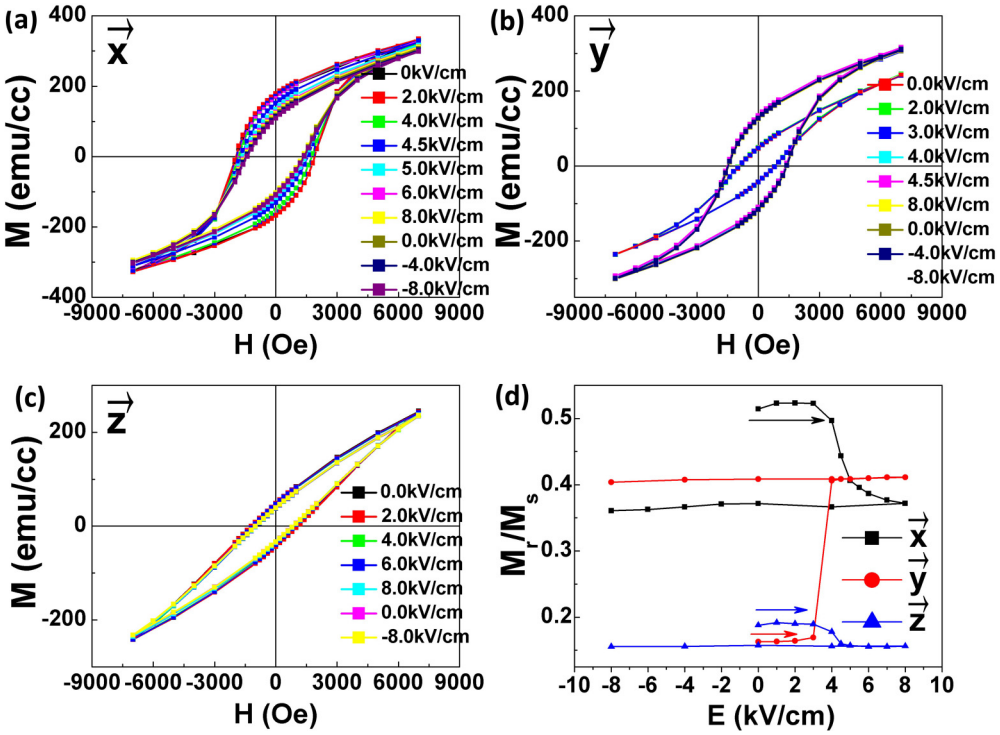

FIG. 3. (Color online) M-H loops of CFO/PMN-PT under different E along (a) $\vec{x}$, (b) $\vec{y}$, and (c) $\vec{z}$. (d) M_r/M_s ratio as a function of E.

Thus, a complete domain I $\rightarrow$ domain II transformation would result in a compressive strain of $\frac{a-c}{c} = -1.3$ % along $\vec{y}$ and a tensile strain of $\frac{\sqrt{a^2+c^2}-\sqrt{2}a}{\sqrt{2}a} = 0.64$ % along $\vec{x}$.

Figure 2 shows the evolution of the XRD line scan with E for the PMN-38PT substrates. The as-grown substrates had six equivalent polarization orientations: four belonging to domain II and two belonging to domain I. In Fig. 2, the intensity of the (101) peak corresponding to domain II can be seen to be stronger than that of the (110) peak for $E = 0$ kV/cm. In this case, we determined that the domain ratio (domain I/domain II) was $R_d = 0.74$. Theoretically, in the unpoled state, $R_d = 0.5$ because the domain distribution should be equivalent among the six possible orientations. However, the different domains may have different x-ray line profiles; accordingly, R_d is only quasilinear with the peak intensity ratio. Here, for simplicity, we used the peak intensity ratio to estimate R_d. With increasing E, a domain I $\rightarrow$ domain II transformation began to be evident near $E = 3$ kV/cm. An abrupt decrease of R_d to a value of 0.159 was then observed over a modest field range of $3.5 \leq E \leq 4$ kV/cm. The abrupt nature indicates a burst of domain reorientations. This decrease was irreversible, as the changes in R_d remained stable upon removal of E [Fig. 2(b)]. Thus, a large remnant strain change can be anticipated. Interestingly, the value of R_d did not change with reversal of the sign of E, indicating that the polarization is confined to the four domain II directions after the initial reorientation and that subsequently only 180° domain switching was induced by E.

Figure 3 shows the M-H loops of a CFO/PMN-PT heterostructure under various applied electric fields. CFO is known to have a negative magnetostriction along both ⟨011⟩ and ⟨100⟩.[10] Along $\vec{x}$, a tensile strain was induced by E in PMN-PT. As a consequence, magnetic domain switching became easier as demonstrated by reductions in H_c and M_r with increasing E. Along $\vec{y}$, a compressive strain was induced in the substrate by E, which was then transmitted to the CFO film. Accordingly, magnetic domain switching became more difficult, as demonstrated by increases in both H_c and M_r with increasing E. Figure 3(d) summarizes the values of the remnant-to-saturation magnetization ratio $R_M = M_r/M_s$ as a function of E-applied out-of-plane. For the CFO film, the value of the ratio is $R_M = 0.16$ in the original state along $\vec{y}$, which increased to $R_M \approx 0.4$ for $E > 4$ kV/cm. The value of R_M was largest along $\vec{x}$ with $R = 0.51$ in the initial state, which then decreased to $R_M < 0.4$ for $E > 5$ kV/cm. The value of R_M along $\vec{y}$ became larger than that along $\vec{x}$ for $E > 5$ kV/cm, indicating a rotation of the magnetic easy axis from $\vec{x}$ to $\vec{y}$. Moreover, it is obvious that the change of R_M along $\vec{y}$ was much larger than that along $\vec{x}$. This is in accordance with the calculated larger strain value along $\vec{y}$ than along $\vec{x}$: i.e., $|-1.3\%| > |0.667|$. The value of R_M along $\vec{z}$ was small over the entire measurement range of $-8 < E < 8$ kV/cm, reflecting a

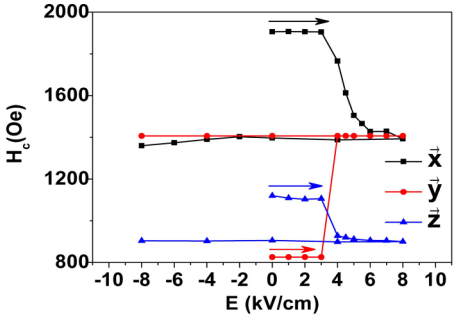

FIG. 4. (Color online) Magnetic coercive field of the CFO film under different E along the $\vec{x}$, $\vec{y}$, and $\vec{z}$ directions.

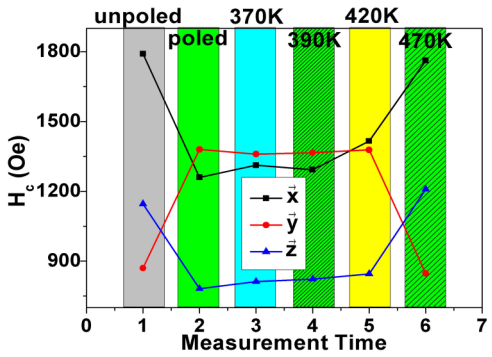

FIG. 5. (Color online) Electric field and thermal annealing dependence of H_c along different directions.

difficulty in altering the magnetic shape anisotropy due to the CFO thin film architecture. Finally, for all three orientations, the changes in the R_M values were stable after removal of E.

Figure 4 shows the evolution of H_c with increasing E for $0 < E < 8$ kV/cm. The value of H_c along $\vec{x}$ decreased from 1.9 to 1.4 kOe; along $\vec{y}$, it increased from 0.8 to 1.4 kOe; and along $\vec{z}$, it decreased from 1.1 to 0.9 kOe. The change in the value of H_c along $\vec{y}$ ($\Delta H_c = 1.4 - 0.8 = 0.6$ kOe) was larger than that along $\vec{x}$ ($\Delta H_c = 1.9 - 1.4 = 0.5$ kOe). This is in consistent with both larger E-induced strains and M_r/M_s ratio changes along $\vec{y}$ (Fig. 3(d)). In addition, the changes in H_c were irreversible upon removal of E along all three directions, indicating stable remnant changes.

Figure 5 illustrates the controllability of H_c for different poling and thermal annealing conditions. Along $\vec{y}$, the value of H_c was 870 Oe for the as-grown CFO/PMN-PT heterostructure, which then increased to 1380 Oe after poling of the substrate. The heterostructure was then annealed at different temperatures (T_a), and the value of H_c was remeasured. For $T_a \leq 420$ K, H_c remained stable. However, the original value of H_c was recovered after annealing at 470 K due to the recovery of the unpoled substrate condition. The Curie temperature of the PMN-38PT substrate was $T_c \approx 450$ K, as determined by dielectric constant data as a function of temperature (see the Supplemental Material[30]). Thus, it is reasonable to conclude that the original value of H_c was not recovered until heating above the $T \rightarrow C$-phase transformation of the substrate. This temperature of $T_a = 470$ K required for H_c recovery in the CFO/PMN-PT heterostructure is notably lower than that previously required for other HAMR medias: e.g., $CoPt_3$ (600 K), FePt (750 K), FePd (760 K), and CoPt (840 K).[9] Accordingly, the coercive field of a CFO/PMN-PT heterostructure might easily be recovered by a HAMR writing head. As an example, consider a bit recorded along $\vec{x}$. Here, CFO has large values of H_c and M_r; thus, the original magnetic state is quite stable. During writing, the local value of H_c would be notably decreased due to a field-induced strain in the substrate; thus, a small magnetic field could switch the magnetization. A laser could then be used to heat the switched area, recovering the large H_c and M_r values. This would facilitate high-density magnetic recording and ease the read-out procedure. There are two main advantages of the proposed E-controlled H_c magnetic recording (EHMR) compared with traditional HAMR: (1) lower energy consumption due to the smaller Curie temperature of piezoelectric substrate compared with that of the ferromagnetic thin films (470 < 600 K) and (2) smaller writing time because the recording unit cells always stay in the ferromagnetic state. Thus, the writing magnetic field does not have to be retained during cooling process, whereas in traditional HAMR, the writing magnetic field has to be stabilized until the memory cell transfers from a paramagnetic to a ferromagnetic state. Considering the economy factors, piezoelectric thin films, instead of piezoelectric single crystal substrates, have to be used in EHMR. Catalan *et al.* reported ferromagnetic domains with a size of ~50 nm for $PbTiO_3$ (PTO) thin film on $DyScO_3$ substrate.[31] Based on our previous results about the relationship of domain size to PMN-PT concentration,[32] it is highly possible that we can obtain much smaller ferroelastic domains in PMN-38PT films compared with pure PTO films. Xu *et al.* used neutron scattering to study the correlation length of polar nanoregions, where a typical size smaller than 10 nm was observed.[33] Therefore, the recording density is confined by the sizable electrode but the domain size of the ferroelastic domains is not. A recording density well exceeding 6 Tb/in.^{2} can be achieved if each domain (10×10 nm) can be used to record 1 bit of information.

Table I summaries the value of the magnetic coercive field changes (ΔH_c) under different electric fields in various ferromagnetic/ferroelectric heterostructures.[34–39] The largest value of ΔH_c previously reported was 50 Oe for Fe_3O_4/PZN-PT.[34] The value for CFO/PMN-38PT, reported here, is more than 10 times larger, i.e., 580 Oe. Three reasons can be identified for the abnormally large value of ΔH_c for CFO/PMN-38PT: (1) the magnetostriction of CFO is more than 10 times larger than that of the previously selected ferromagnetic materials, (2) the T-phase PMN-38PT provides much larger strain compared with that of BTO or rhombohedral PMN-PT substrates, and (3) high-temperature deposition engenders an epitaxial interface between CFO and PMN-PT, which assures an effective elastic strain transfer from substrate to thin film.

IV. CONCLUSIONS

We have fabricated CFO/PMN-38PT epitaxial magnetoelectric heterostructures. Electric fields applied along the out-of-plane direction induced a uniaxial strain in PMN-38PT

TABLE I. Magnetic coercive field tunability in various ferromagnetic/ferroelectric heterostructures.

Thin film Substrate	Ni BTO	Fe BTO	Ni PMN-PT	$Ni_{80}Fe_{20}$ PZN-PT	Fe_3O_4 PZN-PT	Fe_3O_4 PMN-PT	CFO PMN-PT
Magnetostriction (ppm)	−32.9	−7	−32.9	−10.7	20	28	−590
Thickness (nm)	10	10	10	10/100	~500	~900	~400
ΔH_c (Oe)	~10	~25	~30	~13/~0	~50	<30	580

via polarization reorientation, which was then elastically transferred to the CFO films. Large stable changes in the magnetic coercive field of $\Delta H_c \approx 580$ Oe was found along the in-plane 100 direction upon removal of E. The original condition and properties of the heterostructures were recovered after annealing at 470 K. These findings demonstrate effective electric and thermal control of the magnetic coercive field, which might be of potential application in high-density magnetic recording and spintronics.

ACKNOWLEDGMENT

This paper was supported by US Department of Energy (Grant No. DE-FG02-06ER46290).

*Corresponding author: zgwang@vt.edu

[1]X. Gao, L. Liu, B. Birajdar, M. Ziese, W. Lee, M. Alexe, and D. Hesse, Adv. Funct. Mater. **19**, 3450 (2009).
[2]D.-H. Kim, D. E. Nikles, D. T. Johnson, and C. S. Brazel, J. Magn. Magn. Mater. **320**, 2390 (2008).
[3]S. D. Bader, Rev. Mod. Phys. **78**, 1 (2006).
[4]S. H. Sun, H. Zeng, D. B. Robinson, S. Raoux, P. M. Rice, S. X. Wang, and G. X. Li, J. Am. Chem. Soc. **126**, 273 (2004).
[5]P. Oswald, O. Clement, C. Chambon, E. Schouman-Claeys, and G. Frija, Magn. Reson. Imag. **15**, 1025 (1997).
[6]K. Raj and R. Moskowitz, J. Magn. Magn. Mater. **85**, 233 (1990).
[7]A. Hutlova, D. Niznansky, J. L. Rehspringer, C. Estournes, and M. Kurmoo, Adv. Mater. **15**, 1622 (2003).
[8]L. Zhu, S. Nie, K. Meng, D. Pan, J. Zhao, and H. Zheng, Adv. Mater. **24**, 4547 (2012).
[9]M. H. Kryder, E. C. Gage, T. W. McDaniel, W. A. Challener, R. E. Rottmayer, G. Ju, Y.-T. Hsia, and M. F. Erden, Proc. IEEE **96**, 1810 (2008).
[10]Z. Wang, Y. Li, R. Viswan, B. Hu, V. G. Harris, J. Li, and D. Viehland, ACS Nano **7**, 3447 (2013).
[11]W. A. Challener, C. Peng, A. V. Itagi, D. Karns, W. Peng, Y. Peng, X. Yang, X. Zhu, N. J. Gokemeijer, Y. T. Hsia, G. Ju, R. E. Rottmayer, M. A. Seigler, and E. C. Gage, Nat. Photon. **3**, 220 (2009).
[12]L. J. Swartzendruber, G. E. Hicho, H. D. Chopra, S. D. Leigh, G. Adam, and E. Tsory, J. Appl. Phys. **81**, 4263 (1997).
[13]J. Wang, J. Ma, Z. Li, Y. Shen, Y. Lin, and C. W. Nan, J. Appl. Phys. **110**, 043919 (2011).
[14]R. F. L. Evans, R. W. Chantrell, U. Nowak, A. Lyberatos, and H. J. Richter, Appl. Phys. Lett. **100**, 102402 (2012).
[15]B. X. Xu, Z. J. Liu, R. Ji, Y. T. Toh, J. F. Hu, J. M. Li, J. Zhang, K. D. Ye, and C. W. Chia, J. Appl. Phys. **111**, 07B701 (2012).
[16]J.-M. Hu, Z. Li, L.-Q. Chen, and C.-W. Nan, Nat. Comm. **2**, 553 (2011).
[17]M. Liu, O. Obi, J. Lou, Y. Chen, Z. Cai, S. Stoute, M. Espanol, M. Lew, X. Situ, K. S. Ziemer, V. G. Harris, and N. X. Sun, Adv. Funct. Mater. **19**, 1826 (2009).
[18]J. Lou, M. Liu, D. Reed, Y. Ren, and N. X. Sun, Adv. Mater. **21**, 4711 (2009).
[19]A. E. Renault, H. Dammak, G. Calvarin, P. Gaucher, and M. P. Thi, J. Appl. Phys. **97**, 044105 (2005).
[20]D. J. Franzbach, Y. J. Gu, L. Q. Chen, and K. G. Webber, Appl. Phys. Lett. **101**, 232904 (2012).
[21]Y. P. Guo, H. S. Luo, T. H. He, H. Q. Xu, and Z. W. Yin, Jpn. J. Appl. Phys. **41**, 1451 (2002).
[22]Z. Wang, Y. Wang, W. Ge, J. Li, and D. Viehland, Appl. Phys. Lett. **103**, 132909 (2013).
[23]D. Viehland and J. F. Li, J. Appl. Phys. **92**, 7690 (2002).
[24]Y. Kadota and T. Morita, Jpn. J. Appl. Phys. **51**, 09LE08 (2012).
[25]Y. Kadota, H. Hosaka, and T. Morita, J. Korean Phys. Soc. **57**, 902 (2010).
[26]W. Eerenstein, M. Wiora, J. L. Prieto, J. F. Scott, and N. D. Mathur, Nat. Mater. **6**, 348 (2007).
[27]A. Benayad, G. Sebald, L. Lebrun, B. Guiffard, S. Pruvost, D. Guyomar, and L. Beylat, Mater. Res. Bull. **41**, 1069 (2006).
[28]Z. Wang, L. Yan, Y. Yang, J.-F. Li, J. Das, A. L. Geiler, A. Yang, Y. Chen, V. G. Harris, and D. Viehland, J. Appl. Phys. **109**, 034102 (2011).
[29]J. Y. Li and D. Liu, J. Mech. Phys. Solid. **52**, 1719 (2004).
[30]See Supplemental Material at http://link.aps.org/supplemental/10.1103/PhysRevB.89.035118 for the dielectric constant versus temperature results and crystal lattice parameter calculation based on XRD peaks.
[31]G. Catalan, A. Lubk, A. H. G. Vlooswijk, E. Snoeck, C. Magen, A. Janssens, G. Rispens, G. Rijnders, D. H. A. Blank, and B. Noheda, Nat. Mater. **10**, 963 (2011).
[32]F. M. Bai, J. F. Li, and D. Viehland, J. Appl. Phys. **97**, 054103 (2005).
[33]G. Xu, G. Shirane, J. R. D. Copley, and P. M. Gehring, Phys. Rev. B **69**, 064112 (2004).
[34]M. Liu, O. Obi, Z. Cai, J. Lou, G. Yang, K. S. Ziemer, and N. X. Sun, J. Appl. Phys. **107**, 073916 (2010).
[35]S. Gepraegs, A. Brandlmaier, M. Opel, R. Gross, and S. T. B. Goennenwein, Appl. Phys. Lett. **96**, 142509 (2010).
[36]M. Liu, O. Obi, J. Lou, S. Li, X. Xing, G. Yang, and N. X. Sun, J. Appl. Phys. **109**, 07D913 (2011).
[37]T. Wu, A. Bur, K. Wong, J. L. Hockel, C.-J. Hsu, H. K. D. Kim, K. L. Wang, and G. P. Carman, J. Appl. Phys. **109**, 07D732 (2011).
[38]T. Wu, A. Bur, P. Zhao, K. P. Mohanchandra, K. Wong, K. L. Wang, C. S. Lynch, and G. P. Carman, Appl. Phys. Lett. **98**, 012504 (2011).
[39]S. Sahoo, S. Polisetty, C. G. Duan, S. S. Jaswal, E. Y. Tsymbal, and C. Binek, Phys. Rev. B **76**, 092108 (2007).